Available online at www.sciencedirect.com
ScienceDirect
Trans. Nonferrous Met. Soc. China 32(2022) 1981−1993
Transactions of Nonferrous Metals Society of China
www.tnmsc.cn

Pt-decorated $NiWO_4/WO_3$ heterostructure nanotubes for highly selective sensing of acetone

Yong-ping CUI, Ya-ru SHANG, Rui-xia SHI, Quan-de CHE, Jun-peng WANG

School of Materials Science and Engineering, University of Jinan, Jinan 250022, China

Received 28 May 2021; accepted 30 December 2021

Abstract: The heterostructured $NiWO_4/WO_3$ nanotubes (Ni/W NTs) were synthesized by using a facile self-assembly method on the sacrificial polystyrene (PS) nanofibers templates. Then, the Pt-decorated $NiWO_4/WO_3$ (Pt@Ni/W) composite NTs were obtained through using an ultrasonic mixing method. The experimental results display that the order of gas-sensing performance is Pt@Ni/W>Ni/W>WO_3. The 2wt.%Pt@Ni/W-5 NTs indicate the supreme acetone-sensing response (R_{air}/R_{gas}=58.4 at 100×10^{-6}) at 375 °C, which is 10.6 and 1.53 times that of the WO_3 and $NiWO_4/WO_3$ NTs, respectively. Additionally, the 2wt.%Pt@Ni/W-5 NTs also exhibit the dramatically high selectivity toward acetone against ethanol, methanal, methanol, NH_3 and toluene. The Pt-decorated Ni/W NTs show the excellent responsivity and stability toward acetone, which is ascribed to the construction of heterostructured $NiWO_4/WO_3$ and the spill-over effect of Pt nanoparticles.

Key words: $NiWO_4/WO_3$ nanotubes; Pt nanoparticles; gas sensing; acetone; mechanism

1 Introduction

It is crucial to explore a facile and convenient real-time monitoring method to detect toxic and exhaust gases for the environmental protection and human health. For instance, acetone (CH_3COCH_3), as one of the hazardous volatile organic compounds (VOCs), is generally used as raw materials or organic solvent in labs or industries [1−3]. However, it can directly damage the central nervous system, throat, even kidney and liver [4,5]. Therefore, it is imperative to accurately monitor concentration of acetone in the air and decrease the interference from other VOCs.

Recently, various gas sensors, such as electrochemical [6], solid electrolyte [7], catalytic combustion [8] and semiconductor metal oxide (SMO) type [9,10], have been widely used in the industrial and domestic environment. Among these gas sensors, one-dimensional (1D) SMO materials have drawn much attention due to their direct gas path, high aspect ratio and low grain boundary obstacles [11,12].

It is well-known that electrospinning technique, as one of the most versatile and cost-effective approaches, is widely used for the synthesis of 1D materials in large quantities [13−15]. Thus, many oxides including nickel oxide (NiO) [16], tin dioxide (SnO_2) [17], and tungsten oxide (WO_3) [18], have been fabricated by electrospinning method for using as gas sensors. Among the materials, WO_3 has been regarded as one of the fascinating gas sensing materials due to its high reactivity with various VOCs. Nevertheless, 1D WO_3 electrospun nanofibers (NFs) have still suffered from poor selectivity and low response [19].

Thus far, there are all kinds of effective approaches, such as catalyst decoration, morphology and microstructure control and doping,

Corresponding author: Rui-xia SHI, Tel: +86-531-89736225, E-mail: mse_shirx@ujn.edu.cn
DOI: 10.1016/S1003-6326(22)65924-7

to improve the gas-sensing performance of 1D WO_3-based materials [20,21]. For example, ZHANG et al [22] fabricated NiO−WO_3 composite NFs with different NiO contents via electrospinning technique followed by calcination process. Their results demonstrated that the 3mol.%NiO−WO_3 NFs possess superior sensitivity. LIU et al [23] prepared porous WO_3 nanotubes (NTs) through a facile scarified template method. Through introducing an organic compound (3-aminopropyl-triethoxysilane, APTES) on the surface of WO_3 NTs, the as-designed sensor exhibited a highly enhanced response toward NO_2. KIM et al [24] synthesized catalyst-loaded WO_3 NFs with the hierarchically interconnected porosity. Pt nanoparticles (NPs) were encapsulated in a protein nanocage (apoferritin), which enabled uniform catalyst sensitization on the surface of WO_3 NFs. Consequently, the Pt-loaded porous WO_3 NFs showed excellent sensitivity and selectivity toward acetone. The porous and hollow structures dramatically facilitate the promotion of gas accessibility and surface area of materials.

Hence, the 1D porous and hollow $NiWO_4/WO_3$ (Ni/W) NTs were successfully achieved after complete removal of electronspun polystryrene (PS) fiber templates by calcination process. The Pt-decorated Ni/W (Pt@Ni/W) NTs were fabricated by an ultrasonic method. The gas-sensing performance of WO_3, Ni/W and Pt@Ni/W NTs was investigated. The results indicate that the acetone-sensing performance of Pt@Ni/W NTs is greatly better than that of WO_3 and Ni/W NTs. Additionally, the mechanism of enhanced gas-sensing properties was explored.

2 Experimental

2.1 Materials

All reagents were of analytical grade and used without further purification. Ammonium metatungstate hydrate ($(NH_4)_6H_2W_{12}O_{40}\cdot xH_2O$, AMT), and polystryrene (M_r=350000) were supplied by Macklin company. Nickel acetate ($Ni(CH_3COO)_2$) and N,N-dimethyl formamide (DMF) were fabricated by Sinopharm Chemical Reagent Co., Ltd. Polyvinylpyrrolidone (PVP, M_r = 10000) was obtained from Aladdin Industrial Inc. Ethylene glycol (EG) and chloroplatinic acid hexahydrate ($H_2PtCl_6\cdot 6H_2O$) were purchased from Sigma-Alarich. Absolute ethyl alcohol (EtOH) was produced from Tianjin Fuyu Limited Liability Company, China.

2.2 Synthesis of $NiWO_4/WO_3$ nanotubes

The Ni/W NTs were fabricated by a facile template method. Firstly, the PS fibers were prepared using electrospinning technology. 2.2 g PS was added into 8 mL DMF, forming the precursor solution. The solution was drawn into a 10 mL plastic syringe for electrospinning after 12 h stirring. The constant DC voltage and the nozzle- collector distance were 15 kV and 20 cm, respectively. Then, ultralong PS NFs were obtained. Secondly, different molar ratios of AMT and $Ni(CH_3COO)_2$ were dissolved into 2 mL deionized water. Subsequently, the EtOH with different volumes to the 2 mL deionized (DI) water was added into the above aqueous solution. Then, the resulting solution was dropped on the PS fibers until it was fully soaked. After 120 min, the soaked PS fibers were rinsed with EtOH and dried at 60 °C for 10 h. Finally, the dried PS fibers were calcined at 500 °C for 3 h in air with a heating rate of 2 °C/min. According to the different molar ratios of Ni to W, the synthesized NTs were noted as Ni/W-4, Ni/W-5, and Ni/W-6, respectively. Detailed preparation processes are shown in Table 1.

Table 1 Preparation conditions of Ni/W NTs with different molar ratios of Ni to W

Sample	Molar ratio of Ni to W	Mass of AMT/g	Mass of $Ni(CH_3COO)_2$/g
Pure WO_3 NTs	0	0.9700	0.0000
Ni/W-4 NTs	4:100	0.9700	0.0395
Ni/W-5 NTs	5:100	0.9700	0.0494
Ni/W-6 NTs	6:100	0.9700	0.0593

2.3 Preparation of Pt nanoparticles

The Pt NPs with size of 3.5−10 nm were prepared by the polyol reduction method. At first, the solvent EG (4.5 mL) was heated to 150 °C. At the same time, 60 mg of $H_2PtCl_6\cdot 6H_2O$ was dissolved into 0.5 mL of EG. Then, the $H_2PtCl_6\cdot 6H_2O$/EG was introduced dropwise into the heated EG using a syringe. In order to control the morphology of Pt NPs, 0.05 g of PVP in 2 mL of EG was added into the above solution, and the

reaction was carried out at 150 °C for 1 h. The as-prepared NPs were finally cleaned in 35 mL of acetone. The as-resulting Pt NPs were collected using a centrifuge (3000 r/min, 5 min), and the supernatant was discarded afterwards. Finally, the Pt NPs were cleaned in deionized water four times, and redispersed in 30 mL of EtOH to get a uniform dispersion of NPs. The concentration of the obtained Pt NPs is calculated as about 0.75 g/L.

2.4 Fabrication of Pt-decorated $NiWO_4/WO_3$ nanotubes

To obtain the Pt@Ni/W NTs, 5.5 mg of Ni/W-5 NTs were dispersed in 300 μL of ethanol and followed by sonication for 5 min. The as-prepared Pt-NPs solutions of 75, 150 and 225 μL were mixed with the above suspension using sonication for 1 min, respectively. According to the calculated values, the obtained samples are defined as 1wt.%Pt@Ni/W-5 NTs, 2wt.%Pt@Ni/W-5 NTs and 3wt.%Pt@Ni/W-5 NTs, respectively.

2.5 Materials characterization

The morphologies and chemical compositions of samples were analyzed by scanning electron microscope (SEM, QUANTA−250 FEG) and energy dispersive spectrometer (EDS), respectively. The crystal structures of obtained samples were characterized by a powder X-ray diffractometer (XRD, D8-ADVANCE, Bruker Corporation) with a Cu K_α (λ=0.15418 nm) radiation source. The transmission electron microscopic (TEM) and high-resolution transmission electron microscopic (HRTEM) images were performed on a JEOL JEM−2100F with an acceleration voltage of 200 kV. The surface elements were investigated by X-ray photoelectron spectroscopy (XPS, Thermo Scientific Escalab Xi^+).

2.6 Evaluation of gas-sensing performance

The gas sensing performances of the samples were evaluated using CGS−4TPS apparatus with Ag−Pd interdigitated electrodes (Beijing Elite Tech Co., Ltd. of China). The as-prepared samples were mixed with several drops of deionized water. Then, they were coated onto the Ag−Pd electrode. To obtain stable sensor, the electrodes were aged at 200 °C for 2 h. Subsequently, the sensors were placed in a 1.8 L test chamber to adjust the work temperature from room temperature to 450 °C. Finally, the gas responses of sensors were tested through liquid injection of target gas into the chamber using micro-syringe. The relative humidity was regulated ranging from 40% to 45%. The gas-sensing response value is described as R_{air}/R_{gas}, where R_{air} and R_{gas} are the resistance of sensors in air and in target gas, respectively.

3 Results and discussion

3.1 Synthesis of Pt-decorated $NiWO_4/WO_3$ NTs using sacrificial template method

Figure 1 presents the fabrication processing of Pt-decorated $NiWO_4/WO_3$ NTs. Firstly, the PS fibers as sacrificial templates were prepared through electrospinning method (Step I). Then, the as-collected PS fibers were soaked in the EtOH solution of Ni/W precursor (Step II). The Ni/W NTs were obtained by calcination of resulting-nanofibers (Step III). The Pt NPs were prepared by a facile polyalcohol process. At last, the Pt NPs were decorated on the surface of Ni/W NTs using an ultrasonic method (Step IV).

3.2 Microstructure and chemical analysis

The SEM images of Ni/W-4 NTs are presented in Fig. 2. It can be found that Ni/W-4 is

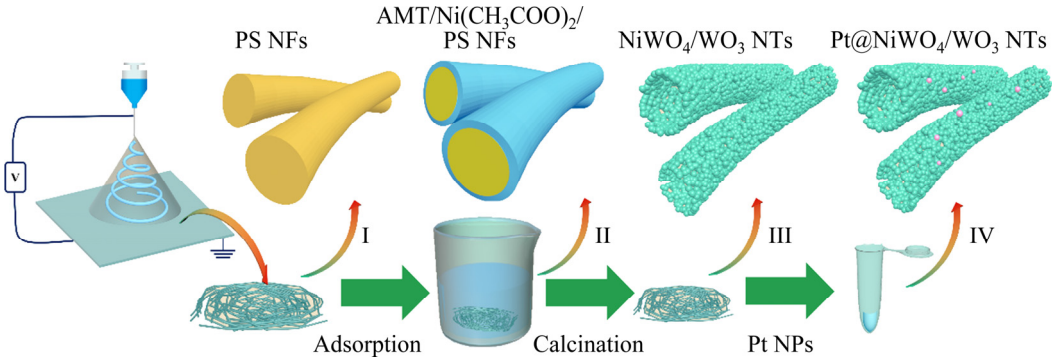

Fig. 1 Synthesis schematic illustration of Pt@Ni/W NTs

tubular in shape. The wall thickness of Ni/W-4 NTs varies with the volume ratio of DI water to EtOH. When the volume ratio of the DI water to EtOH is 1:6 (12 mL EtOH), the Ni/W-4 NTs show rough surface and relatively uniform diameter in the range of 1.42−2.21 μm (Fig. 2(a)). And it can be observed that the PS fiber template has been absolutely removed, and the wall thickness of NTs is about 400 nm (Fig. 2(b)). Increasing the volume ratio to 1:8, the NTs have a uniform diameter in the range of 1.39−2.14 μm and a wall thickness of 370 nm (Figs. 2(c) and (d)). Further increasing the volume ratio to 1:10, the wall thickness is almost unchanged but the diameter of NTs becomes nonuniform (Figs. 2(e) and (f)). And some cracks on the surface of NTs are observed. According to the above analysis, it can be known that the diameter of Ni/W-4 NTs is uniform and the wall thickness of Ni/W-4 NTs is small when the volume ratio of DI water to EtOH is 1:8.

Accordingly, the molar ratio of Ni to W was further adjusted from 4:100 to 5:100 and 6:100 by keeping the volume ratio of DI water to EtOH at 1:8. Meanwhile, the WO_3 NTs were also fabricated through the same volume ratio as a control sample. As shown in Fig. 3, it can be found that the WO_3 NTs are composed of uniform nanoparticles (Fig. 3(a)). When the molar ratio of Ni to W was increased from 4:100 to 5:100, the diameter of the Ni/W-5 and Ni/W-4 NTs is 1.39−2.32 μm (Fig. 3(b)).

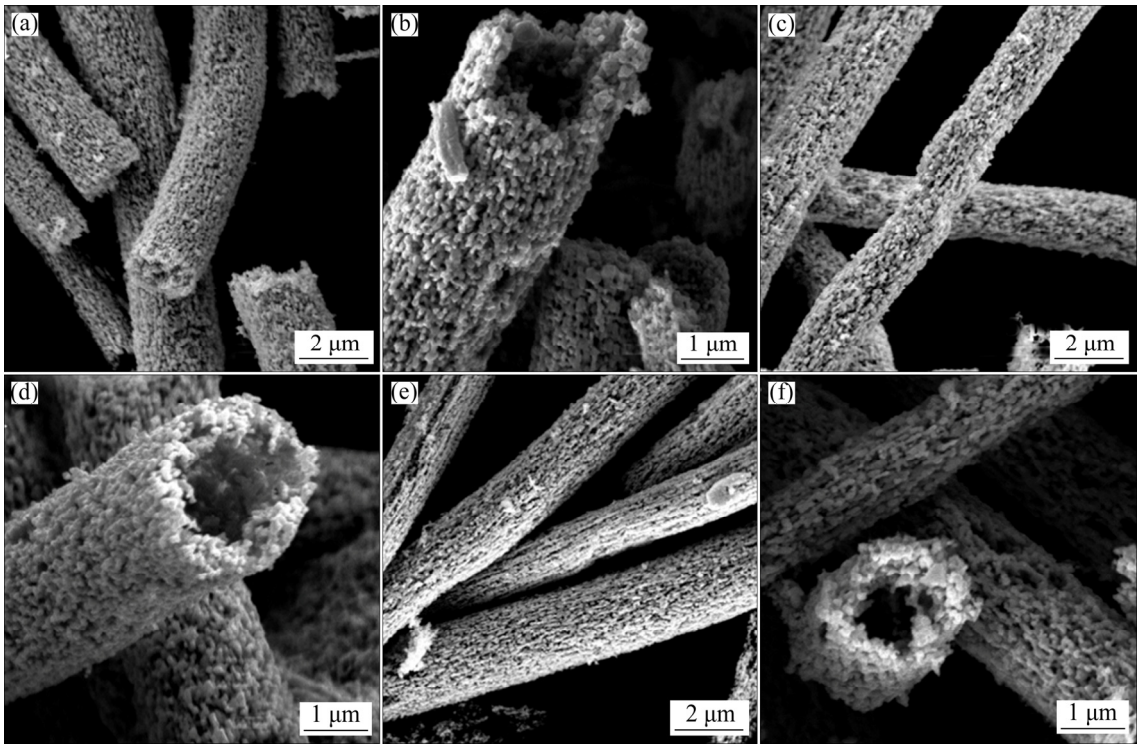

Fig. 2 SEM images of obtained Ni/W-4 NTs prepared with different volume ratios of Ni/W precursor solution to EtOH: (a, b) 1:6; (c, d) 1:8; (e, f) 1:10

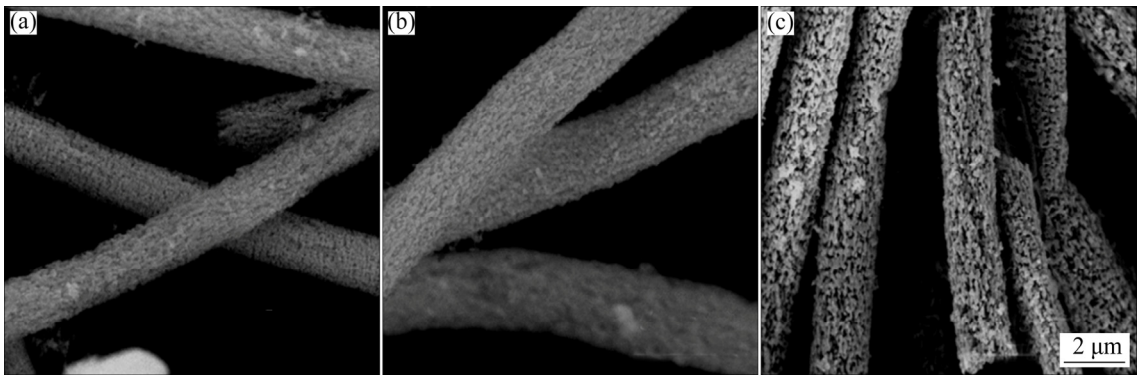

Fig. 3 SEM images of WO_3 (a), Ni/W-5 (b) and Ni/W-6 (c) NTs

Compared with the Ni/W-4 NTs (Fig. 2(c)), the nanoparticles consisting of the NTs is more uniform. Further increasing the molar ratio of Ni to W to 6:100, many particles appear on the surfaces of Ni/W-6 NTs (Fig. 3(c)). The microstructures become loose but it is worth to noting that many nanoparticles agglomerate (Fig. 3(c)). Later, the morphology transformation resulted from the molar ratio of Ni to W is also verified by the results of sensing response of the NTs (Fig. 8(a)).

Hence, to further improve the performance of Ni/W NTs, the Pt nanoparticles were decorated on the Ni/W-5 NTs by classical polyol reduction method. The SEM images of Pt@Ni/W-5 NTs with various mass fractions of Pt are shown in Fig. 4. The morphologies of 1wt.%Pt@Ni/W-5 (Fig. 4(a)) and 2wt.%Pt@Ni/W-5 (Fig. 4(b)) NTs are same as that of Ni/W-5 NTs. Figure 4(c) exhibits that the 3wt.%Pt@Ni/W-5 NTs still retain a tubular structure but there are some big pores on their surfaces (Fig. 4(c)). The Pt nanoparticles are too small to be observed (Figs. 4(d, e)) [19,22]. However, the EDS elemental mapping (Fig. 4(f)) of 2wt.%Pt@Ni/W NTs demonstrates the existence of Pt, Ni, W and O elements and high dispersibility of Pt nanoparticles.

The crystalline characteristics of 2wt.%Pt@-Ni/W-5 NTs were investigated by HRTEM. As shown in Figs. 5(a) and (b), the tubular structure of sample cannot be observed through TEM image due to the thick wall of nanotube. The lattice spacings of 3.67 and 2.86 Å are attributed to the (200) plane of m-WO_3 and $(\bar{1}11)$ plane of $NiWO_4$ crystal, respectively (Fig. 5(c)), which is also confirmed by XRD analysis (corresponding to the blue circle of Fig. 5(b)). Moreover, Fig. 5(d) reveals that the (111) plane of Pt is identified with the interplanar distance of 2.28 Å, confirming the presence of Pt NPs.

Figure 6 illustrates the XRD results of the WO_3, Ni/W-5 and 2wt.%Pt@Ni/W-5 NTs. All samples are agreement with the monoclinic WO_3 (m-WO_3, JCPDS No. 80-0950). There are three main characteristic diffraction peaks observed at 2θ = 23.12°, 23.58° and 24.37°, which can be well matched with the (002), (020) and (200) lattice planes of m-WO_3, respectively [25]. It exhibits characteristic peaks at 19.2°, 30.9° and 36.6° for Ni/W-5, which correspond to (100), $(\bar{1}11)$ and (002) lattice planes of $NiWO_4$ (JCPDS No. 72-0480), respectively [26].

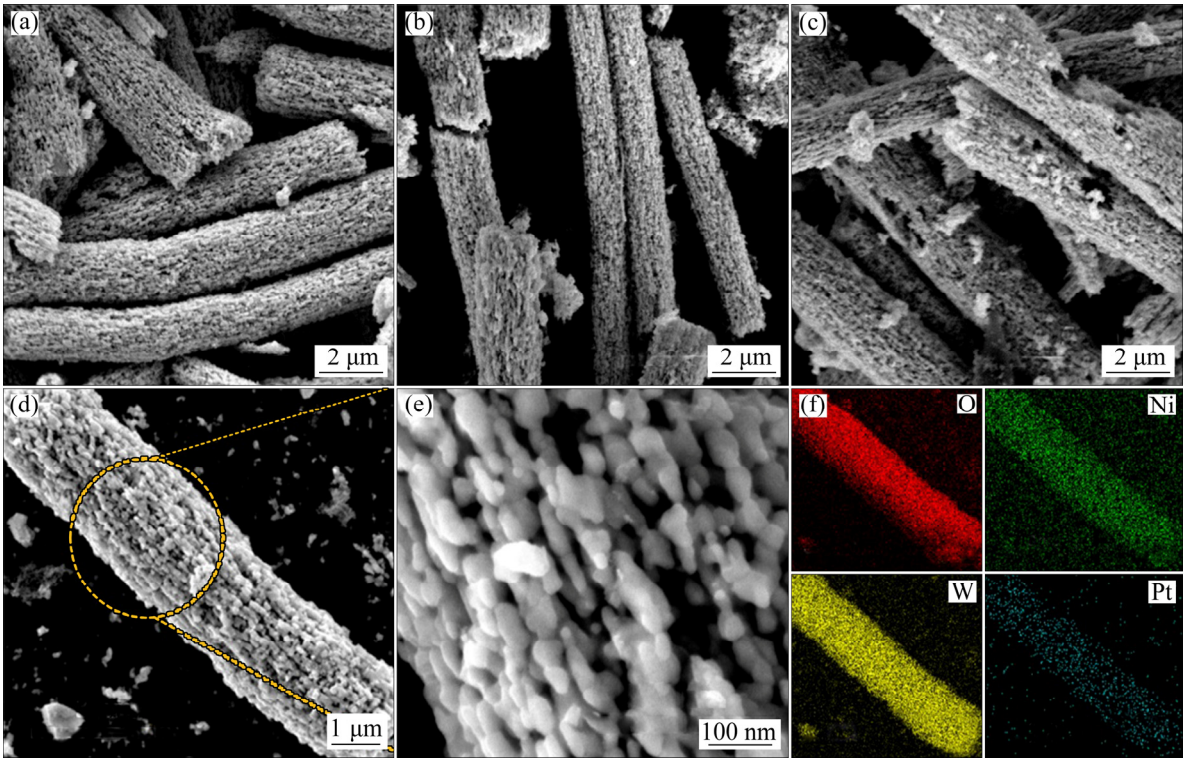

Fig. 4 SEM images of Pt@Ni/W-5 NTs with different Pt contents: (a) 1 wt.%; (b) 2 wt.%; (c) 3wt.%; (d, e) Enlarged image of (b); (f) Corresponding EDS elemental mapping of (d)

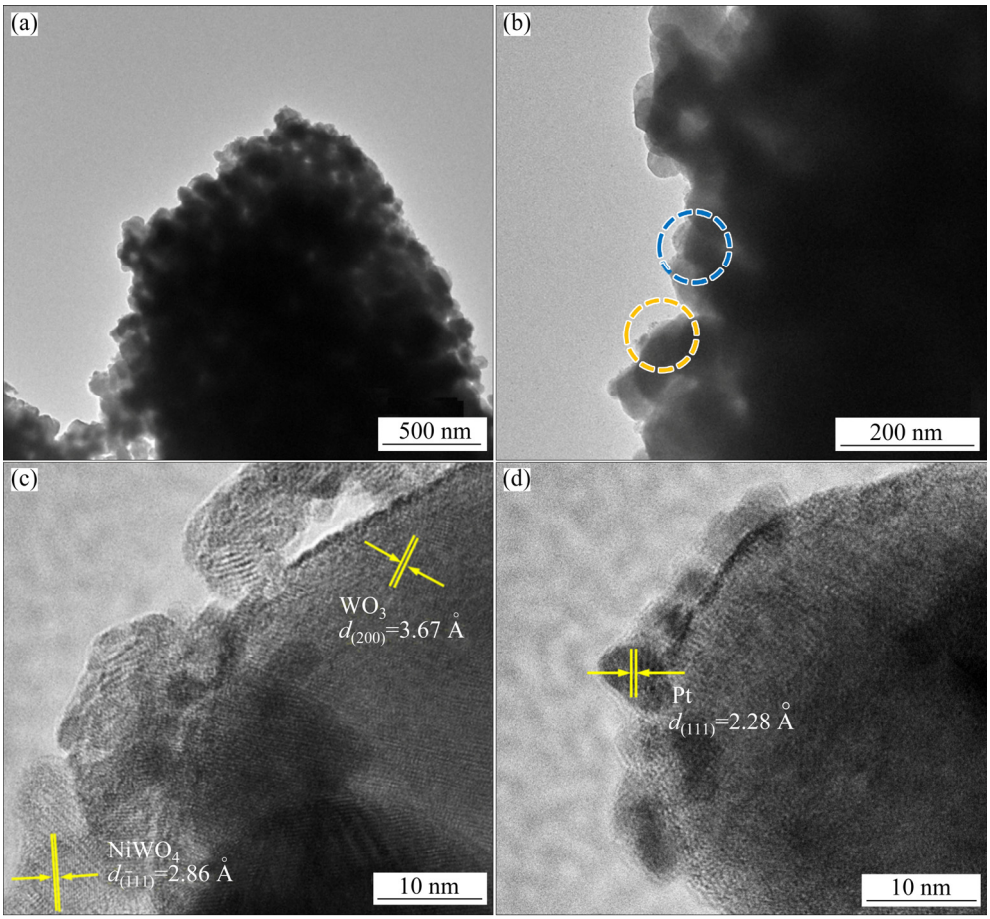

Fig. 5 TEM images (a, b) and HRTEM images (c, d) of 2wt.%Pt@Ni/W-5 NTs

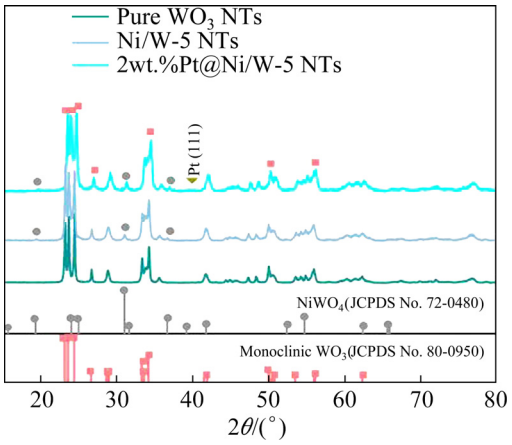

Fig. 6 XRD patterns of WO_3, Ni/W-5 and 2wt.%Pt@-Ni/W-5 NTs

However, there is a weak characteristic peak at 39.3° corresponding to the (111) lattice plane of Pt in 2wt.%Pt@Ni/W-5 NTs due to loading of small amounts of catalysts.

The chemical composition and electronic state of 2wt.%Pt@Ni/W-5 NTs were tested using XPS analysis. Figure 7(a) shows the survey scans of the XPS, confirming the existence of Ni, O, Pt and W elements in the 2wt.%Pt@Ni/W-5 NTs. The fine spectrum of O 1s is shown in Fig. 7(b), exhibiting a single asymmetric peak at 530.1 eV. The peak can be deconvoluted to two oxygen species in the 2wt.%Pt@Ni/W-5 NTs, which are fitted to approximately 529.3 and 530.4 eV, corresponding to lattice oxygen (O 1) and surface chemisorbed oxygen (O 2), respectively [25]. As shown in Fig. 7(c), the high-resolution spectra of W 4f have two peaks at 35.7 and 37.9 eV, matching with the binding energy of W $4f_{7/2}$ and W $4f_{5/2}$, respectively, which resulted from W^{6+} in WO_3 and $NiWO_4$ [26]. There are two characteristic peaks of Ni $2p_{3/2}$ and Ni $2p_{1/2}$ binding energy located at 854.7 and 878.5 eV, respectively, indicating the main form of Ni^{2+} in the 2wt.%Pt@Ni/W-5 NTs (Fig. 7(d)) [26]. The obtained two characteristic peaks in the Pt 4f high resolution spectra (Fig. 7(e)) at 78.6 and 70.1 eV corresponded to Pt $4f_{5/2}$ and Pt $4f_{7/2}$, respectively, which demonstrated the existence of Pt [27]. Furthermore, the existence of weak peak was estimated at binding energy of 73.6 eV, illustrating the presence of PtO in small amounts.

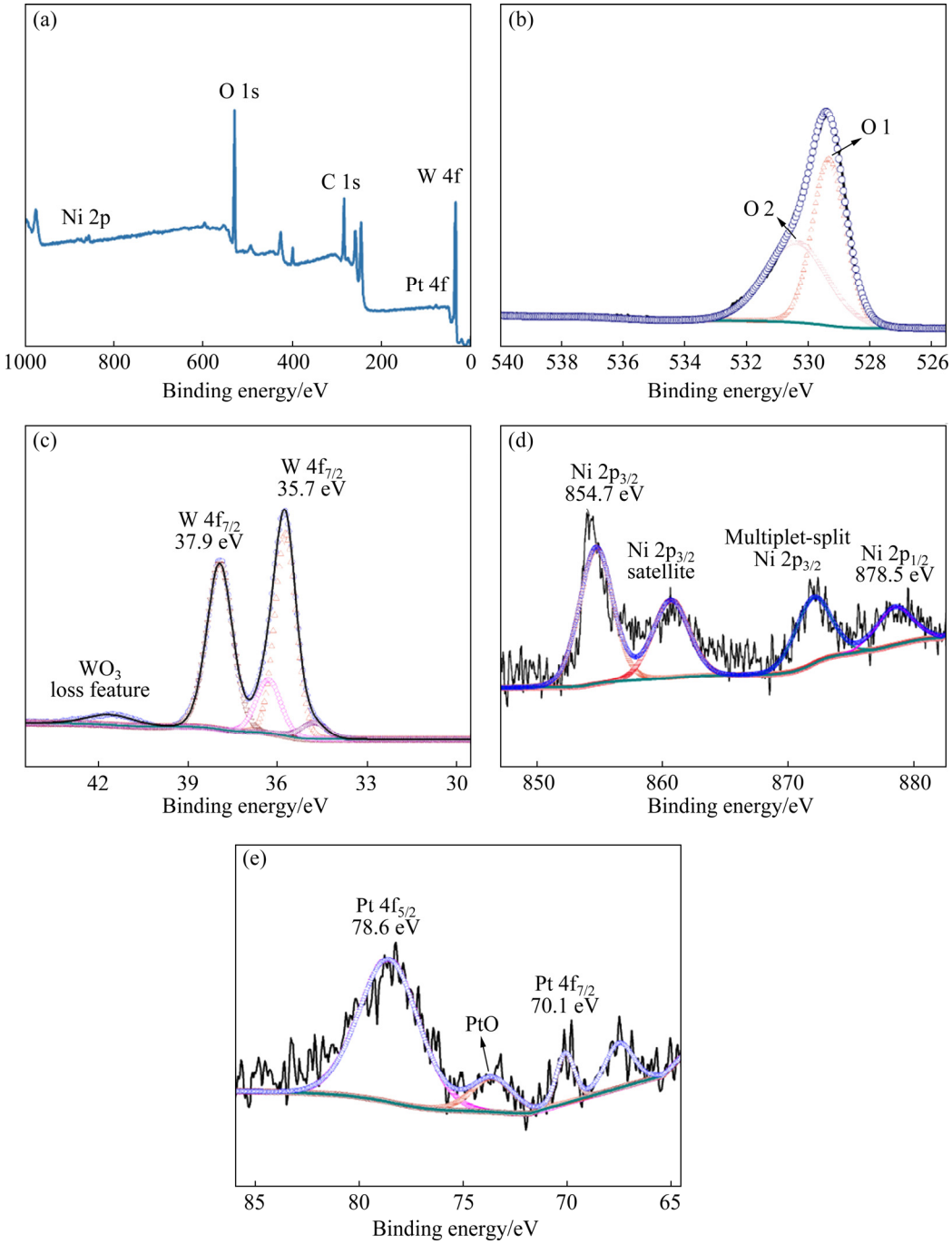

Fig. 7 XPS analysis results of 2wt.%Pt@Ni/W-5 NTs: (a) Full survey spectrum; (b) O 1s; (c) W 4f; (d) Ni 2p; (e) Pt 4f

3.3 Evaluation of gas sensing

Acetone is regarded as one of the most dangerous VOCs. It is urgent to seek for a gas-sensing material with high sensitivity and selectivity toward acetone. The tubular microstructures of samples are beneficial for the sensing materials [12,14]. It is widely accepted that the state of oxygen on the surface of sensing-materials is extremely vital for surficial interaction between chemisorbed oxygen species and target gases, which is temperature dependent. Moreover, it is very significant to adjust the sensitivity of materials and even the selectivity by investigating the operating temperature [25]. Figure 8(a) shows the relationship between working temperature and sensing response towards acetone (100×10^{-6}) for Ni/W NTs with different molar ratios of Ni to W and WO_3 in the range of 250−400 °C. The WO_3 NTs show lower acetone responses (R_{air}/R_{gas}<8.6) at the entire temperatures. The response of Ni/W NTs was

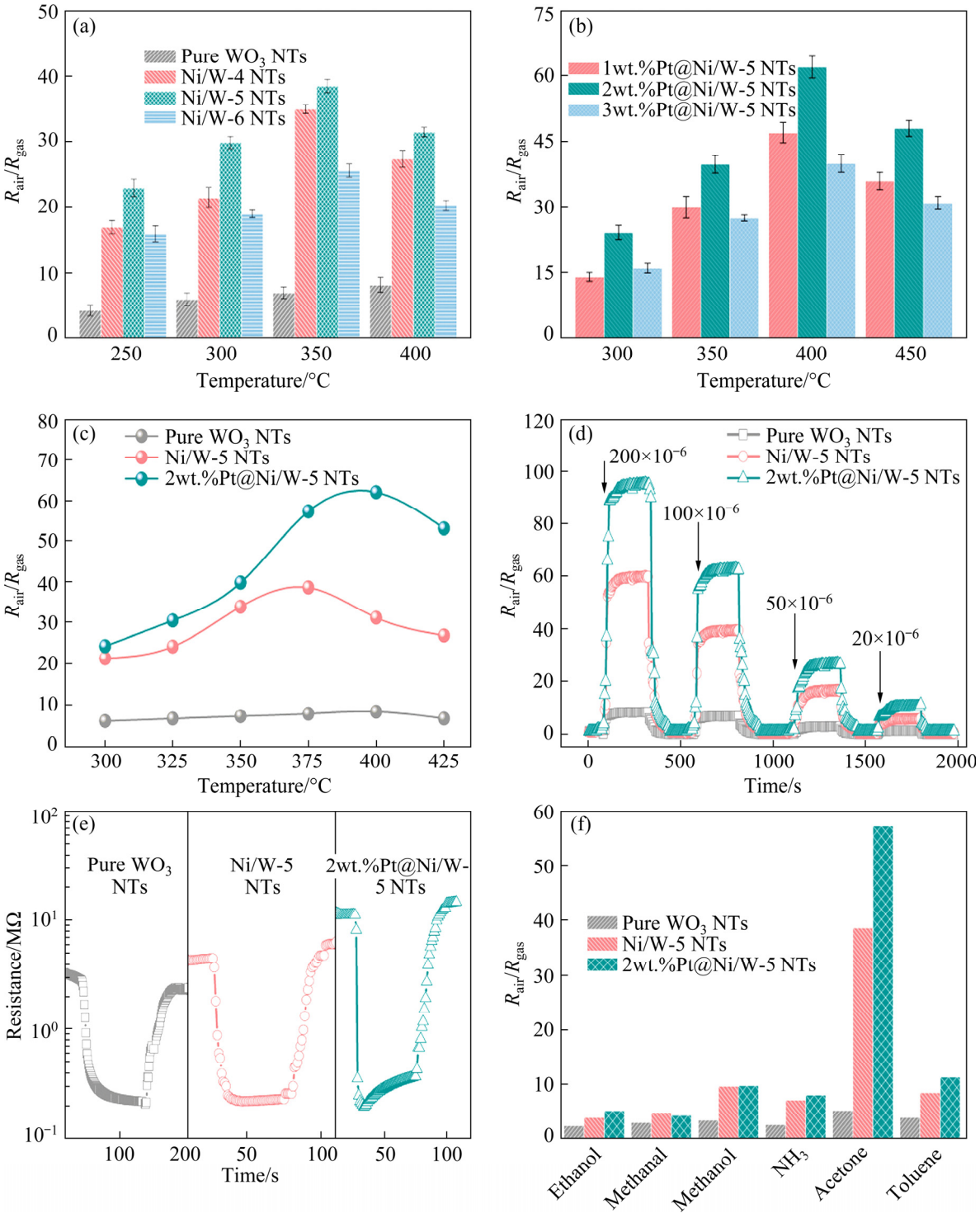

Fig. 8 Temperature dependent measurement toward 100×10^{-6} acetone of samples with different molar ratios of Ni to W and Pt contents (a, b, c), dynamic response transients toward 100×10^{-6} acetone at 375 °C (d), dynamic resistance transients toward 100×10^{-6} acetone at 375 °C (e), and gas selectivity (f)

greatly enhanced. The Ni/W-5 NTs showed better acetone-sensing performance at the entire temperatures than that of Ni/W-4 and Ni/W-6 NTs. And the Ni/W-5 NTs possess the optimized sensor response (R_{air}/R_{gas}) of 38.2 at 350 °C. To evaluate the effects of Pt nanoparticles on the temperature-dependent acetone-sensing performances, the responses of Ni/W-5 decorated with different mass fractions of Pt were investigated in the temperature range of 300−450 °C at 100×10^{-6}

acetone (Fig. 8(b)). The result indicates that the 2wt.%Pt@Ni/W-5 NTs exhibit the highest response of 63.1 at 400 °C. Further comparing the temperature dependency of acetone-sensing characteristics in a temperature range of 300−425 °C, the optimum working temperatures of WO_3, Ni/W-5 and 2wt.%Pt@Ni/W-5 NTs are determined to be 400, 375 and 400 °C, respectively (Fig. 8(c)). It can be seen that the 2wt.%Pt@Ni/W-5 NTs also have the highest response at 375 °C. Additionally, dynamic response transients toward acetone were also carried out at 375 °C in a concentration range of $(20-200)\times10^{-6}$ (Fig. 8(d)). The result demonstrates that 2wt.%Pt@Ni/W-5 NTs exhibit the highest response compared with WO_3 and Ni/W-5 NTs at the entire concentrations. Generally, the higher sensitivity of the sensing materials possesses the shorter response and recovery time. Here, the response and recovery time are defined as the time to reach 90% of the full response (recovery) value of the sensor. At 375 °C, the responses of WO_3, Ni/W-5 and 2wt.%Pt@Ni/W-5 NTs under 100×10^{-6} acetone (Fig. 8(e)) are calculated as 18, 11 and 7, respectively. And the recovery time of them is 31, 24 and 19 s, respectively.

Selectivity of gas sensor materials is also a critical sensing parameter for accurate detection of VOCs. As displayed in Fig. 8(f), the selective response performances of WO_3, Ni/W-5 and 2wt.%Pt@Ni/W-5 NTs were investigated toward various gases (100×10^{-6}) at working temperature of 375 °C. The results show that 2wt.%Pt@Ni/W-5 NTs exhibit the dramatically high selectivity toward acetone (R_{air}/R_{gas}=58.4 at 100×10^{-6}), which is 5.9−12.3 times higher than those to 100×10^{-6} ethanol, methanal, methanol, NH_3 and toluene. The acetone-sensing response (R_{air}/R_{gas}=58.4 at 100×10^{-6}) of 2wt.%Pt@Ni/W-5 NTs at 375 °C is 10.6 and 1.53 times that of WO_3 and Ni/W NTs. The WO_3 shows bad selectivity to various gases.

Based on the above analysis, the sensing stability of 2wt.%Pt@Ni/W-5 NTs toward 100×10^{-6} acetone was explored at 375 °C. It is clear (Fig. 9(a)) that there is no distinct change of the response under six-cycle measurement, which indicates that 2wt.%Pt@Ni/W-5 NTs exhibit the utmost reproducibility and stability. Figure 9(b) shows the corresponding response values as a function of the acetone concentration toward 2wt.%Pt@Ni/W-5 NTs. It could be seen clearly that the response values increased with the increase of acetone concentration. In general, the sensor response and the target gas concentration (C) follow the Eq. (1) [28]:

$$S=1+aC^b \tag{1}$$

where S and a are named as response (R_{air}/R_{gas}) and the pre-exponential factor, respectively. And b is named as the surface species charge parameter, which is usually in the range of 0.5−1 [29]. At a certain temperature, Eq. (1) can be changed into a linear formation as

$$\lg(S-1)=b\lg C+\lg a \tag{2}$$

As shown in the inset of Fig. 9(b), there is a probably linear relationship between lg (S−1) and lg C, suggesting that the sensor response of 2wt.%Pt@Ni/W-5 NTs and acetone concentration follow the Eq. (1).

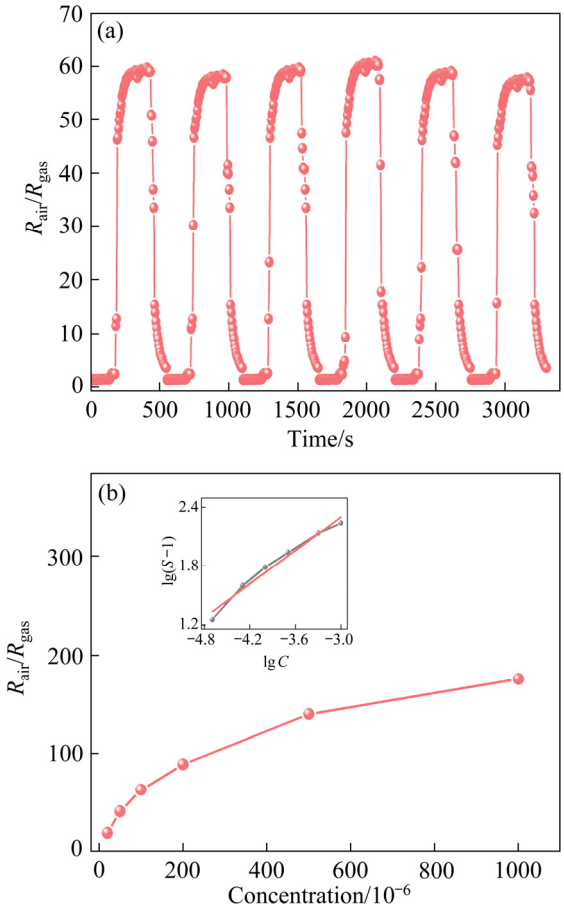

Fig. 9 Sensing stability measurement of 2wt.%Pt@Ni/W-5 NTs toward 100×10^{-6} acetone at 375 °C (a), and corresponding response value as function of acetone concentration toward 2wt.%Pt@Ni/W-5 NTs (b)

3.4 Gas sensing mechanism of Pt-decorated $NiWO_4/WO_3$ NTs

Nowadays, there is no overwhelming mode to reveal the gas chemical sensing performance of inorganic nanomaterials. It is well acknowledged that the sensing mechanism of SMO materials is directly related with the changing resistance that is caused by the adsorption of oxygen active species (O^-, O^{2-} and O_2^-) on the surface of materials [30]. As depicted in Fig. 10(a), when the gas sensors are exposed to air, the oxygen active species are formed on the surface of the WO_3 NTs by transferring the electrons from the conduction band of WO_3 to chemisorbed oxygen, which leads to the resistance increase of sensors due to the generation of an electron depletion layer near the surface of WO_3 NTs. When some reducing gases, such as acetone, are introduced to WO_3 NTs, the adsorbed oxygen adions can be desorbed via surface reaction with acetone [31]. Accordingly, many of captured electrons were released back to the conduction band of WO_3, resulting in a reduction in the resistance of WO_3 NTs. When the sensors are exposed to air, the resistance gets back to the original again.

Herein, 2wt.%Pt@Ni/W-5 NTs exhibit the superior acetone-sensing performances. As shown in Fig. 10(b), the tubular structures of samples facilitate the reaction of surface chemisorbed oxygen with acetone molecules, and the gas molecules can be diffused rapidly in the sensing layer. The increase of oxygen absorption species can cause the widening of electron depletion layer. Especially, what is really needed to point out that is the creation of $NiWO_4/WO_3$ heterostructures. As shown in Fig. 8(e), the resistances in air of the WO_3 and Ni/W-5 NTs are 1.7 and 4.6 MΩ, respectively.

Moreover, like Au, catalytic Pt is well-known chemical sensitizer [32]. Pt can effectively promote the surface reactions by the spill-over effect, which resulted in the dramatic decline in the resistance of sensors during exposure to acetone. Therefore, the surface reactions to selective detection acetone of Pt@Ni/W-5 NTs were enhanced.

To clarify the sensing mechanisms, there is a energy level diagram of 2wt.%Pt@Ni/W-5 NTs (Fig. 10(c)). $NiWO_4$ and WO_3 are both the *n*-type semiconductor [33]. The band gaps (E_g) of $NiWO_4$ and WO_3 are measured to be 2.20 and 2.62 eV, respectively [34]. And the conduction band energies of $NiWO_4$ and WO_3 are calculated to be about −0.45 eV (E_{C2}) and −0.03 eV (E_{C3}) [35]. When $NiWO_4$ and WO_3 are in contact tightly, the electrons will transfer from the lower work function to the higher one. Thus, the potential barriers and energy band bending are constructed near the interface between $NiWO_4$ and WO_3. Similarly, Pt possesses the highest work function (5.36 eV) in all metals [35]. When the semiconductors and the Pt

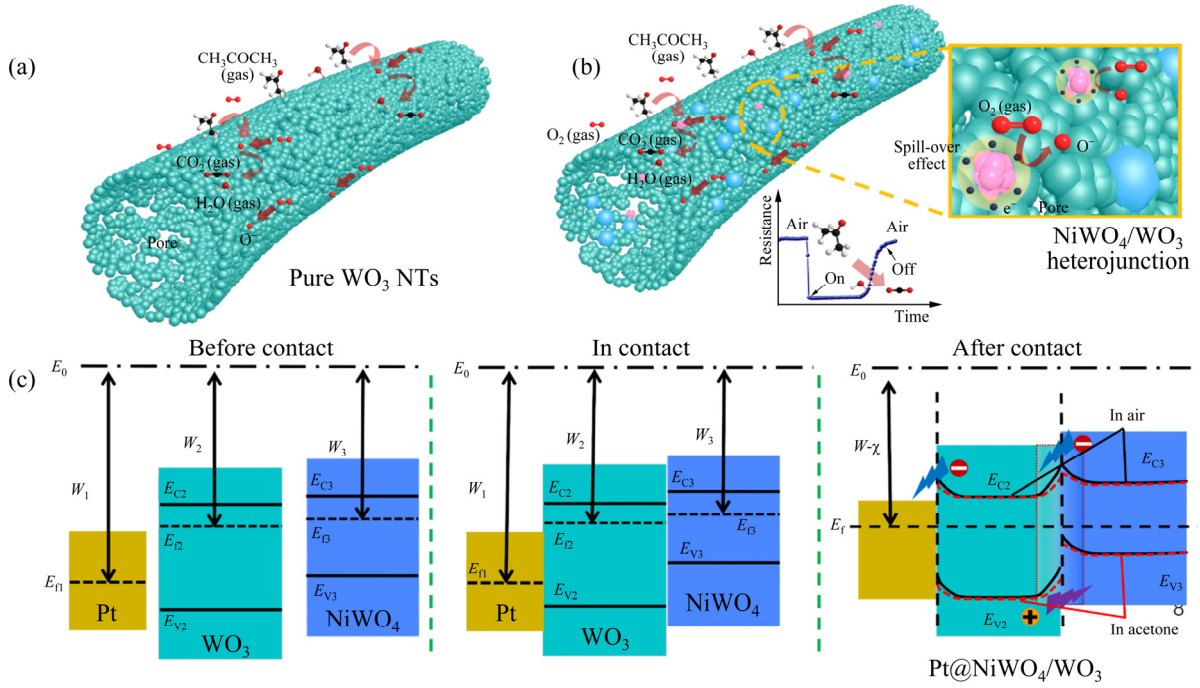

Fig. 10 Schematic illustration of WO_3 NTs (a), enhanced acetone-sensing performance (b), and energy level diagram (c) of Pt@Ni/W NTs

NPs are in contact the Schottky barrier will be established, which means that Pt and WO_3 can capture electrons from $NiWO_4$ when the sensors are exposed to air. Due to the presence of potential barriers, the electrons are confined to $NiWO_4$. The results correspond with the increased resistance of 2wt.%Pt@Ni/W-5 NTs compared with that of the WO_3 NTs.

In addition, when the 2wt.%Pt@Ni/W-5 NTs are exposed to acetone, the adsorption of electron donor on the surface of sensors will contribute to the downward bands bending. The resulting electric field can separate the electron-hole pairs and facilitate the electron transfer to the donor-semiconductor interfaces [36]. Thus, the decreasing potential barriers of sensors promote the electron migration, thereby leading to the excellent acetone-response of 2wt.%Pt@Ni/W-5 NTs.

4 Conclusions

(1) The porous Ni/W NTs were prepared using facile self-assembly on the sacrificial polystyrene (PS) nanofiber templates followed by calcination process.

(2) Pt-decorated porous Ni/W NTs with high sensitivity and selectivity for detecting acetone were fabricated.

(3) The gas sensing properties of 2wt.%Pt@-Ni/W-5 NTs showed dramatic improvement toward acetone.

(4) The 2wt.%Pt@Ni/W-5 NTs possessed the supreme acetone-sensing performance (R_{air}/R_{gas} = 58.4 at 100×10^{-6}) at 375 °C, which is 10.6 and 1.53 times that of WO_3 and Ni/W-5 NTs, respectively.

(5) The enhancement of Pt-decorated porous Ni/W NTs should be attributed to the formation of heterostructured $NiWO_4/WO_3$ and the spill-over effect of Pt NPs.

Acknowledgments

This work was supported by the National Natural Science Foundation of China (Nos. 51772130, 51972145)

References

[1] LI Yan, CHEN Li-li, ZHAO Fang-xian. Highly selective acetone sensor based on ternary Au/Fe_2O_3−ZnO synthesized via co-precipitation and microwave irradiation [J]. Transactions of Nonferrous Metals Society of China, 2018, 28: 137−144.

[2] MENG Gui-fang, XIANG Qun, PAN Qing-yi, XU Jia-qiang. The selective acetone detection based on Fe_3O_4 doped WO_3 nanorods [J]. Sensor Letters, 2011, 9: 128−131.

[3] LI Gao-jie, CHENG Zhi-xuan, XIANG Qun, YAN Liu-ming, WANG Xiao-hong, XU Jia-qiang. Bimetal PdAu decorated SnO_2 nanosheets based gas sensor with temperature-dependent dual selectivity for detecting formaldehyde and acetone [J]. Sensors and Actuators B: Chemical, 2019, 283: 590−601.

[4] ALIZADEH N, JAMALABADI H, TAVOLI F. Breath acetone sensors as non-invasive health monitoring systems: A review [J]. IEEE Sensors Journal, 2020, 20(1): 5−31.

[5] JIAO Wan-li, ZHANG Lei. Preparation and gas sensing properties for acetone of amorphous Ag modified $NiFe_2O_4$ sensor [J]. Transactions of Nonferrous Metals Society of China, 2012, 22: 1127−1132.

[6] YU Hua-liang, WANG Jun, ZHENG Biao, ZHANG Bing-wen, LIU Li-qin, ZHOU Ying-wu, ZHANG Cheng, XUE Xiao-ling. Fabrication of single crystalline WO_3 nano-belts based photoelectric gas sensor for detection of high concentration ethanol gas at room temperature [J]. Sensors and Actuators A: Physical, 2020, 303: 111865−111872.

[7] DONG Cheng-jun, ZHAO Rong-jun, YAO Li-jia, RAN Yan, ZHANG Xu, WANG Yu-de. A review on WO_3 based gas sensors: Morphology control and enhanced sensing properties [J]. Journal of Alloys and Compounds, 2020, 820: 153194−153217.

[8] BHATI V S, HOJAMBERDIEV M, KUMAR M. Enhanced sensing performance of ZnO nanostructures-based gas sensors: A review [J]. Energy Reports, 2020, 6: 46−62.

[9] ZHOU Qu, ZENG Wen, CHEN Wei-gen, XU Ling-na, KUMAR R, UMAR A. High sensitive and low-concentration sulfur dioxide (SO_2) gas sensor application of heterostructure NiO−ZnO nanodisks [J]. Sensors and Actuators B: Chemical, 2019, 298: 126870−126876.

[10] DEY A. Semiconductor metal oxide gas sensors: A review [J]. Materials Science and Engineering B, 2018, 229: 206−217.

[11] WEI Shao-hong, ZHAO Guo-yan, DU Wei-min, TIAN Qing-qing. Synthesis and excellent acetone sensing properties of porous WO_3 nanofibers [J]. Vacuum, 2016, 124: 32−39.

[12] SHANG Ya-ru, CUI Yong-ping, SHI Rui-xia, YANG Ping, WANG Jun-peng, WANG Ying-zi. Regenerated $WO_{2.72}$ nanowires with superb fast and selective adsorption for cationic dye: Kinetics, isotherm, thermodynamics, mechanism [J]. Journal of Hazardous Materials, 2019, 379: 120834.

[13] LIU Wei, XU Lin, SHENG Kuang, ZHOU Xiang-yu, ZHANG Xin-ran, CHEN Cong, DONG Biao, BAI Xue, LU Ge-yu, SONG Hong-wei. Facile synthesis of controllable TiO_2 composite nanotubes via templating route: Highly sensitive detection of toluene by double driving from

Pt@ZnO NPs [J]. Sensors and Actuators, B: Chemical, 2018, 273: 1676−1686.

[14] YAN Xiao-yan, TONG Xi-li, WANG Jian, GONG Chang-wei, ZHANG Min-gang, LIANG Li-ping. Synthesis of hollow nickel oxide nanotubes by electrospinning with structurally enhanced lithium storage properties [J]. Materials Letters, 2014, 136: 74−77.

[15] KIM S, PARK S, PARK S, LEE C M. Acetone sensing of Au and Pd-decorated WO_3 nanorod sensors [J]. Sensors and Actuators B: Chemical, 2015, 209: 180−185.

[16] KHALIL A, HASHAIKEH R. Electrospinning of nickel oxide nanofibers: Process parameters and morphology control [J]. Materials Characterization, 2014, 95: 65−71.

[17] ZHANG Xue-ying, XU Guo-gang, WANG Hui-yong, CUI Hong-zhi, ZHAN Xiao-yuan, WANG Xin-zhen. Enhanced acetone sensing properties of hollow SnO_2 fibers using poplar catkins as a bio-template [J]. Powder Technology, 2019, 344: 183−189.

[18] LENG Ji-yan, XU Xiu-juan, LV Ning, FAN Hui-tao, ZHANG Tong. Synthesis and gas-sensing characteristics of WO_3 nanofibers via electrospinning [J]. Journal of Colloid and Interface Science, 2011, 356: 54−57.

[19] GUO Xian-zhi, KANG Yan-fei,YANG Tai-li,WANG Shu-rong. Low-temperature NO_2 sensors based on polythiophene/WO_3 organic-inorganic hybrids [J]. Transactions of Nonferrous Metals Society of China, 2012, 22: 380−385.

[20] KIM D H, JUNG J W, CHOI S J, JANG J S, KOO W T, KIM I D. Pt nanoparticles functionalized tungsten oxynitride hybrid chemiresistor: Low-temperature NO_2 sensing [J]. Sensors and Actuators B: Chemical, 2018, 273: 1269−1277.

[21] YANG Xiao-jiao, SALLES V, KANETI Y V, LIU Min-su, MAILLARD M, JOURNET C, JIANG Xu-chuan, BRIOUDE A. Fabrication of highly sensitive gas sensor based on Au functionalized WO_3 composite nanofibers by electrospinning [J]. Sensors and Actuators B: Chemical, 2015, 220: 1112−1119.

[22] ZHANG Jin-niu, LU Hong-bing, LIU Chang, CHEN Chu-jun, XIN Xia. Porous NiO−WO_3 heterojunction nanofibers fabricated by electrospinning with enhanced gas sensing properties [J]. RSC Advances, 2017, 7: 40499−40509.

[23] LIU Wei, XU Lin, SHENG Kuang, CHEN Cong, ZHOU Xiang-yu, DONG Biao, BAI Xue, ZHANG Shuang, LU Ge-yu, SONG Hong-wei. APTES-functionalized thin-walled porous WO_3 nanotubes for highly selective sensing of NO_2 in a polluted environment [J]. Journal of Materials Chemistry A, 2018, 6: 10976−10989.

[24] KIM D H, JANG J S, KOO W T, CHOI S J, KIM S J, KIM I D. Hierarchically interconnected porosity control of catalyst-loaded WO_3 nanofiber scaffold: Superior acetone sensing layers for exhaled breath analysis [J]. Sensors and Actuators B: Chemical, 2018, 259: 616−625.

[25] KOO W T, CHOI S J, KIM N H, JANG J S, KIM I D. Catalyst-decorated hollow WO_3 nanotubes using layer-by-layer self-assembly on polymeric nanofibre templates and their application in exhaled breath sensor [J]. Sensors and Actuators B: Chemical, 2016, 223: 301−310.

[26] MANCHEVA M N, IORDANOVA R S, KLISSURSKI D G, TYULIEV G T, KUNEV B N. Direct mechanochemical synthesis of nanocrystalline $NiWO_4$ [J]. The Journal of Physical Chemistry C, 2007, 111: 1101−1104.

[27] KHAN H, RIGAMONTI M G, BOFFITO D C. Enhanced photocatalytic activity of Pt−TiO_2/WO_3 hybrid material with energy storage ability [J]. Applied Catalysis B: Environmental, 2019, 252: 77−85.

[28] BAO Meng, CHEN Yu-jiao, LI Fang, MA Jian-min, LV Ting, TANG Yun-jing, CHEN Li-bao, XU Zhi, WANG Tai-hong. Plate-like p-n heterogeneous NiO/WO_3 nanocomposites for high performance room temperature NO_2 sensors [J]. Nanoscale, 2014, 6: 4063−4066.

[29] FENG Xiao-yang, CHEN Yu-bin, QIN Zhi-xiao, WANG Meng-long, GUO Lie-jin. Facile fabrication of sandwich structured WO_3 nanoplate arrays for efficient photoelectrochemical water splitting [J]. ACS Applied Materials and Interfaces, 2016, 8: 18089−18096.

[30] DONG Peng-yu, HOU Gui-hua, XI Xin-guo, SHAO Rong, DONG Fan. WO_3-based photocatalysts: Morphology control, activity enhancement and multifunctional applications [J]. Environmental Science: Nano, 2017, 4: 539−557.

[31] PARK J, YOON H, CHOI S Y, SON J W. Nanoscaffold WO_3 by kinetically controlled polymorphism [J]. Crystal Growth and Design, 2019, 19: 479−486.

[32] ZHU Jing, LI Wen-zhang, LI Jie, LI Yao-min, HU Hai-shi, YANG Ya-hui. Photoelectrochemical activity of $NiWO_4$/WO_3 heterojunction photoanode under visible light irradiation [J]. Electrochimica Acta, 2013, 112: 191−198.

[33] CHOI S J, KIM S J, CHO H J, JANG J S, LIN Y M, TULLER H L, RUTLEDGE G C, KIM I D. WO_3 nanofiber-based biomarker detectors enabled by protein-encapsulated catalyst self-assembled on polystyrene colloid templates [J]. Small, 2016, 12: 911−920.

[34] MONTINI T, GOMBAC V, HAMEED A, FELISARI L, ADAMI G, FORNASIERO P. Synthesis, characterization and photocatalytic performance of transition metal tungstates [J]. Chemical Physics Letters, 2010, 498: 113−119.

[35] SHIN J W, CHOI S J, YOUN D Y, KIM I D. Exhaled VOCs sensing properties of WO_3 nanofibers functionalized by Pt and IrO_2 nanoparticles for diagnosis of diabetes and halitosis [J]. Journal of Electroceramics, 2012, 29: 106−116.

[36] ZHANG Z, YATES J T Jr. Band bending in semiconductors: Chemical and physical consequences at surfaces and interfaces [J]. Chemical Reviews, 2012, 112: 5520−5551.

对丙酮高气敏选择性的 Pt 纳米颗粒修饰的 $NiWO_4/WO_3$ 异质结构纳米管

崔永平，商亚茹，师瑞霞，车全德，王俊鹏

济南大学 材料科学与工程学院, 济南 250022

摘　要：以聚苯乙烯(PS)纳米纤维为模板，采用简单的自组装法制备异质结构 $NiWO_4/WO_3$(Ni/W)纳米管。采用超声混合法获得 Pt 修饰的 $NiWO_4/WO_3$ 复合纳米管(Pt@Ni/W)。结果表明，气敏性能从高到低依次为 Pt@Ni/W>Ni/W>WO_3。2%Pt@Ni/W-5 纳米管在 375 ℃时对 100×10^{-6} 丙酮具有最高的响应值(58.4)，分别是 WO_3 和 $NiWO_4/WO_3$ 纳米管的 10.6 和 1.53 倍。此外，相比于乙醇、甲醛、甲醇、氨气和甲苯，2%Pt@Ni/W-5 纳米管对丙酮显示出极高的选择性。Pt 修饰的 $NiWO_4/WO_3$ 纳米管对丙酮表现出良好的响应性和稳定性，这归因于 $NiWO_4/WO_3$ 异质结构的形成和 Pt 纳米颗粒的溢出效应。

关键词：$NiWO_4/WO_3$ 纳米管；Pt 纳米颗粒；气敏；丙酮；机理

(Edited by Xiang-qun LI)